Chapter 5

Biomedical image retrieval in NSST domain using shape and texture features

Different biomedical images, X-ray, MRI, ultrasound, CT scan etc. play crucial role in identifying abnormalities in individual's body and their treatment. Furthermore, it plays a significant role for research purposes. Biomedical images contain a variety of information from various bodily areas or specific regions. There are various approaches of representing the diverse details present in biomedical images. There exists feature extraction techniques based on either global information or local information present in images. These global or local descriptors carry complimentary image details where global descriptors represent the overall image as a whole and the local descriptors capture the very minute details present in images. To represent the complicated image details of biomedical images, few works have been done which considers both local and global details.

This chapter presents two different approaches for biomedical image retrieval which considers both shape and texture details present in images.

1. Biomedical image retrieval using ZM and NSST domain maximum of subbands local directional edge pattern
2. Biomedical image retrieval based on shape and singular value decomposition based modelling in NSST domain

5.1 Biomedical image retrieval using ZMs and NSST domain maximum of subbands local directional edge pattern

This section introduces one feature descriptor which is a fusion of local texture and global shape features extracted from biomedical images which enables it to provide effective description of biomedical images with complicated structural and spatial information. In this work, a novel framework called Zernike moments and NSST domain maximum of subbands local directional edge pattern (ZM-NSST-MSLDEP) for retrieval of biomedical images is presented. The ZM-NSST-MSLDEP fuses both image ZM based shape features and non subsampled shearlet transform domain maximum of subbands local directional edge pattern (NSST-MSLDEP) based texture features for retrieval of biomedical images. The global shape feature which provides an overall perspective of an image is integrated with effective local texture features in order to improve the discriminative power of features. The orthogonal low order ZM are extracted from the input spatial image to form the global shape features whereas the local texture features are calculated from the image NSST subbands. Unlike wavelets, the shearlet transform is highly appropriate in describing images containing 2-D singularities. The local texture information is computed from a set of NSST detail subbands present in a scale using directional maximum edge concept. In a given scale, with respect to every reference first the edges in a specific direction is calculated for each detail subband and then based on the magnitude of maximum to minimum distribution of edges of all the subbands, the NSST-MSLDEP value in a specific direction is obtained. At each scale, the NSST-MSLDEP values at $0°, 45°, 90°, 135°, 180°, 225°, 270°, 315°$ directions are calculated. The local textures from the approximation subband is extracted using simple yet powerful uniform LBP and concatenate them with the features obtained from detail subbands.

5.1.1 Methodology

In this section, the ZM and NSST based maximum of subbands local directional edge pattern (ZM-NSST-MSLDEP) computation procedure is explained in details. The functional block diagram of ZM-NSST-MSLDEP based image retrieval framework is shown in Fig. 5.1. The complete ZM-NSST-MSLDEP computation process is divided into a few main steps such as: ZM computation, NSST decomposition, non-linearity addition, encoding of NSST detail subbands using proposed

directional maximum edge based concept i.e NSST-MSLDEP, encoding of NSST approximation subband using simple LBP uniform pattern and final feature vector computation.

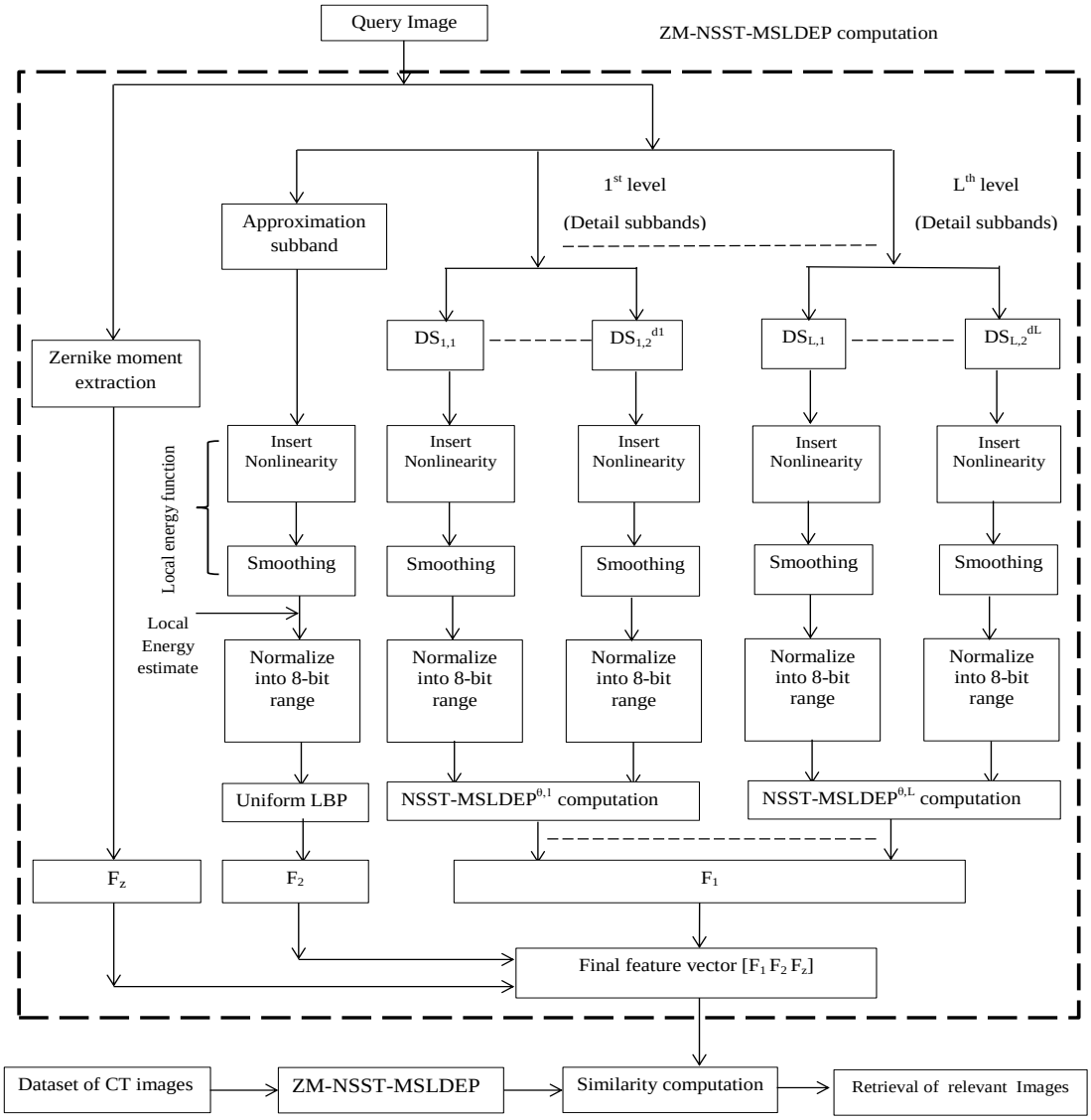

Figure. 5.1: Functional block diagram of ZM-NSST-MSLDEP feature based image retrieval framework

5.1.1.1 Global shape feature extraction using ZM

Shape feature is one of the powerful attribute of the images for a CBIR system. When images are affected by changes in orientation, viewpoint, scale and other factors, shape descriptors that are invariant to these changes become important for effective image retrieval. There are mainly two types of shape descriptors that exist in the literature - contour based and region based [8]. Object shape boundary information is used in contour-based shape descriptors whereas region based

shape descriptors use both object shape boundary and internal region of the shape. Fourier descriptor [26–28], curvature scale space [29], edges and corners of border segments [203, 204] and the techniques presented in [2, 3, 205, 206] are some of the examples of contour and region based shape descriptors. Most commonly used region based shape descriptors are moment-based techniques [5, 30–33].Invariances such as translation, scale, and rotation invariance are not present in geometric moments. Hence, geometric moments cannot be used directly as a shape descriptor for image processing applications. Hu [31] provided a set of seven invariant features over geometric moments which are invariant towards scale, translation and rotation. These invariant features have been used in many applications since then. As the basis set of geometric moments is not orthogonal, information redundancy and computational cost is considerably high. To overcome these issues, Teague [32] proposed to use ZM which is based on the theory of orthogonal polynomials. ZM is invariant to rotation variation, resistant to noise and it can represent image with minimum redundancy. ZMs also possess scale invariant property. ZM performs better compared to other moment based approaches and it can be used in different applications [6, 207, 208]. Lower order ZMs are used by T. Amir et. al [14] to extract shape features for classification of benign and malignant masses. With the help of polar coordinates, the square image is mapped into unit circle. ZM over a unit disk for a function $I(p,q)$ is defined as

$$ZM_{\rho\kappa_z} = \frac{\rho+1}{\pi}\int\int_{p^2+q^2<=1} I(p,q)V^*_{\rho\kappa_z}(p,q)dpdq \tag{5.1}$$

where ρ and κ_z are the order and repetition of the function $I(p,q)$. ρ is a positive integer, $0 \leq \kappa_z \leq \rho$ and $\rho - |\kappa_z|$=even. $V_{\rho\kappa_z}(p,q)$ is the Zernike orthogonal basis function and $V^*_{\rho\kappa_z}(p,q)$ is its complex conjugate.

$$V_{\rho\kappa_z}(p,q) = V_{\rho\kappa_z}(\Upsilon,\Theta) = R_{\rho\kappa_z}(\Upsilon)exp(j\kappa_z\Theta) \tag{5.2}$$

where $\Theta = tan^{-1}(\frac{q}{p})$,$0 \leq \Theta \leq 2\pi$ and $\Upsilon = \sqrt{p^2+q^2}$.

$$R_{\rho\kappa_z}(\Upsilon) = \sum_{s=0}^{(\rho-|\kappa_z|)/2}(-1)^s\frac{(\rho-s)!}{s!(\frac{\rho+|\kappa_z|}{2}-s)!(\frac{\rho-|\kappa_z|}{2}-s)!}(\Upsilon)^{(\rho-2s)} \tag{5.3}$$

$R_{\rho\kappa_z}(\Upsilon)$ is the radial polynomial. The zeroth order approximation of the

ZM is defined as follows

$$ZM_{\rho\kappa_z} = \frac{2(\rho+1)}{\pi N^2} \sum_{t=0}^{N-1} \sum_{u=0}^{N-1} I(p_t, q_u) R_{\rho\kappa_z}(\Upsilon_{tu}) e^{-j\kappa_z \Theta_{tu}} \tag{5.4}$$

where $p_t = \frac{2t+1-N}{N\sqrt{2}}$ and $q_u = \frac{2u+1-N}{N\sqrt{2}}$ is the normalized coordinate pertaining to the location of pixel (t, u) for all $t, u = 0, 1, ...N-1$.

The biomedical images such as CT images comprise of distinct shapes, structural and textural patterns. The ZM's were successfully employed to extract such important structural features [24, 25]. The ZM's are considered as global feature extractors for the reason that they are able to examine and express the content of the full image and derive the statistical information of the pixel distributions inside it. As ZM's are obtained using the procedure of summations, the influence of noise over the magnitude of coefficients is almost minimal. The low order ZM coefficients can express the overall information representation about an image when compared to moments of higher orders. Furthermore the ZM's can extract the shape features with much less no. of features compared to LBP.

Motivated from these reasons, we use ZMs in this work to extract the global shape features. Authors discussed in [25], that the $|ZM_{\rho,\kappa_z}| = |ZM_{\rho,-\kappa_z}|$, hence the ZM with negative κ_z is not considered. The following expression is used to calculate the total number of ZM of order ρ_{max}.

$$T_c = \begin{cases} \frac{1}{4}(\rho_{max}+2)^2 & \text{if} \rho_{max} \text{is even} \\ \frac{1}{4}(\rho_{max}+1)(\rho_{max}+3) & \text{if} \rho_{max} \text{is odd} \end{cases} \tag{5.5}$$

For $\rho_{max} = 5$, $T_c = \frac{1}{4}(5+3)(5+1) = \frac{1}{4}(8 \times 6) = 12$. The Table 5.1 presents the list of lower order ZM considered here.

5.1.1.2 Local texture feature extraction from NSST detail subbands using maximum of subbands local directional edge pattern (NSST-MSLDEP)

While carrying out a L-level NSST decomposition (with d_s, $s \in [1, 2, ...L]$ number of directions from finest to coarsest scale) on an image, a total of 1 approx-

Table 5.1: The list of $ZM_{\rho\kappa_z}$ for order ρ_{max}=5

order $0 \leq \rho \leq \rho_{max}$	Repetition $0 \leq \kappa_z \leq$	$\rho - \kappa_z$	$ZM_{\rho\kappa_z}$	No. of $ZM_{\rho\kappa_z}$ at each ρ	T_c
0	0	0(even)	$ZM_{0,0}$	1	1
1	1	0(even)	$ZM_{1,1}$	1	2
2	0	2(even)	$ZM_{2,0}$	2	4
	1	1(odd)			
	2	0(even)	$ZM_{2,2}$		
3	0	3(odd)	-	2	6
	1	2(even)	$ZM_{3,1}$		
	2	1(odd)	-		
	3	0(even)	$ZM_{3,3}$		
4	0	4(even)	$ZM_{4,0}$	3	9
	1	3(odd)	-		
	2	2(even)	$ZM_{4,2}$		
	3	1(odd)	-		
	4	0(even)	$ZM_{4,4}$		
5	0	5(odd)	-	3	12
	1	4(even)	$ZM_{5,1}$		
	2	3(odd)	-		
	3	2(even)	$ZM_{5,3}$		
	4	1(odd)	-		
	5	0(even)	$ZM_{5,5}$		

imation and $2^{d_1}, 2^{d_2}.....2^{d_{L-2}}, 2^{d_{L-1}}, 2^{d_L}$ number of detail subbands are obtained at $1, 2....., L-2, L-1, L$ scales respectively.

In an n^{th} subband in a given scale $s \in [1, 2, ...L]$, the edge information w.r.t each reference/centre in a given direction $\theta \in [0°, 45°, 90°, 135°, 180°, 225°, 270°, 315°]$ is obtained using (5.6)

$$D_{\theta,s,n} = \xi^{R+1}_{\theta,s,n} - \xi^{R}_{\theta,s,n} \tag{5.6}$$

where $\xi^{R+1}_{\theta,s,n}$ and $\xi_{\theta,s,n}$ are normalized energy values at $R+1^{th}$ and R^{th} radius respectively.

After calculating all the subband edge values in θ direction in scale s, the maximum to minimum subband edge distribution is achieved from the magnitude of 2^{d_s} number of NSST subband's directional edge values (5.7).

$$M_i(x,y) = \underset{M}{arg}(max^i(|D_{\theta,s,1}(x,y)|, |D_{\theta,s,2}(x,y)|, ... \left|D_{\theta,s,2^{d_L}}(x,y)\right|)) \tag{5.7}$$

where $max^i(p)$ computes the i^{th} maximum location in the 'p' array.

Then the NSST-MSLDEP maps are computed in each scale ($s \in [1, ..., L]$) in 8 different directions utilizing the sign of directional edges (5.8)

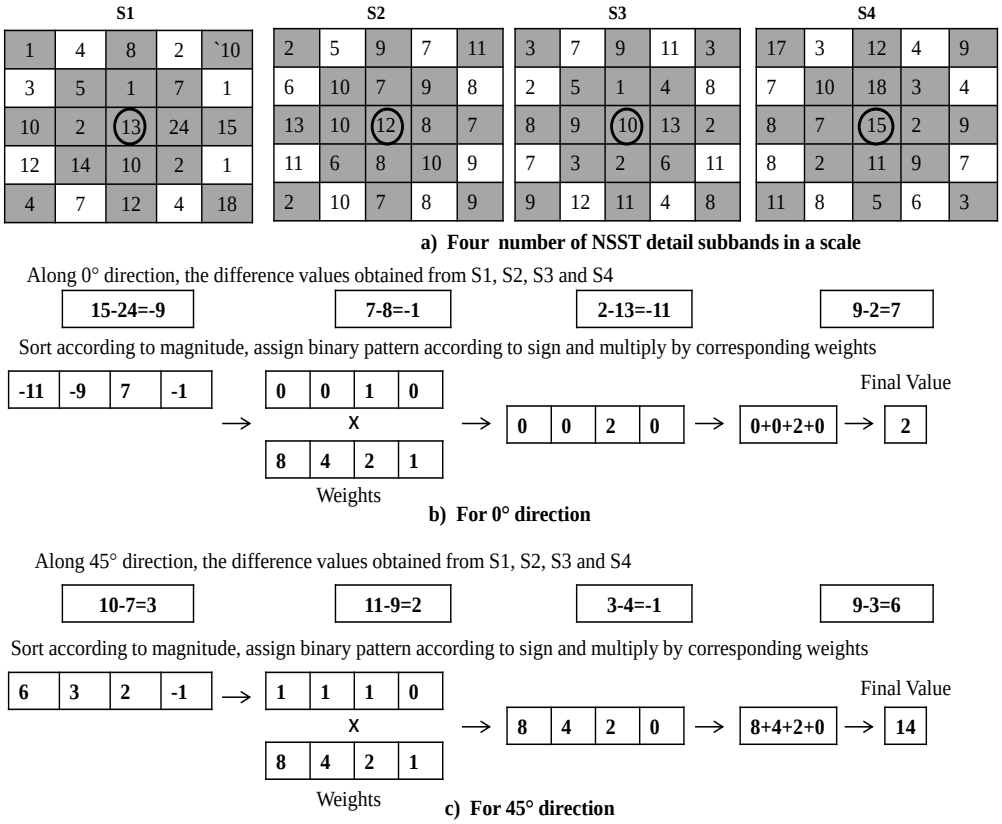

Figure. 5.2: Sample example of NSST-MSLDEP computation in two directions

$$NSST - MSLDEP^{\theta,s}(x,y) = \sum_{i=1}^{2^{d_s}} 2^{(d_s - i)}.f(D_{\theta,s,M_i}(x,y)) \tag{5.8}$$

where

$$f(x) = \begin{cases} 1 & if\ x \geq 0 \\ 0 & else \end{cases}$$

Finally, the range of values in feature maps at various directions θ will depend on the d_L no. of directions at each scale which was set initially for NSST image decomposition.

The histogram for $NSST-MSLDEP^{\theta,s}$ in a given direction (θ) and scale (s) is calculated using (5.9)

$$H_{NSST-MSLDEP^{\theta,s}}(l) = \sum_{x=1}^{R}\sum_{y=1}^{C} f_2(NSST - MSLDEP(x,y), l); \quad L \in [0, (2^{d_s} - 1)] \tag{5.9}$$

In case of a L-level NSST decomposition with d_s ($s \in [1, 2, ...L]$) number of directions from finest to coarsest scale, the histogram of feature maps for all 8 directions from all the scales can be expressed using the feature vector F_1:

$$F_1 = \begin{bmatrix} H_{NSST-MSLDEP^{0^\circ},1} & ..... & H_{NSST-MSLDEP^{315^\circ},1} \\ H_{NSST-MSLDEP^{0^\circ},2} & ..... & H_{NSST-MSLDEP^{315^\circ},2} \\ . & & \\ . & & \\ . & & \\ H_{NSST-MSLDEP^{0^\circ},L} & ..... & H_{NSST-MSLDEP^{315^\circ},L} \end{bmatrix} \tag{5.10}$$

5.1.1.3 Local texture feature extraction from NSST approximation subband using 'uniform' LBP

LBP[46,192] is computationally simple yet powerful local texture descriptor. LBP captures texture information from images locally. A 3×3 square neighborhood is taken into consideration for each pixel of a grayscale image and a binary pattern is obtained by comparing with the neighbouring pixels.

The example computation of LBP for 3×3 neighborhood is presented in Fig. 5.3. The LBP feature maps contain pattern values in the range of [0-255] out of which only 58 patterns occur frequently representing image curves, edges, flat areas and line ends etc. These 58 pattern values are identified by the presence of maximum '2' bitwise 0/1 transitions in the 8 bit binary pattern. For example '00010000' has '2' 0/1 transitions while '00110010' has '4' 0/1 transitions. The patterns with maximum 2 bit wise transitions are considered as 'uniform' patterns while all the other patterns with more than 2 bit wise transitions are considered as 'non-uniform' patterns and their occurrence is considered in the 59^{th} bin.

The feature vector F_2 is constructed by computing the LBP 'uniform' histogram as described above.

Sample image		
19	23	15
9	10	11
12	8	17

Difference		
9	13	5
-1		1
2	-2	7

Binary code		
1	1	1
0		1
`1	0	1

Weight		
32	64	128
16		1
8	4	2

LBP		
	235	

Figure. 5.3: Example computation of LBP for a 3×3 neighborhood

5.1.1.4 Final feature vector formation

The final feature vector is constructed by concatenating F_1, F_2 and F_Z given by

$$FV = [F_1, F_2, F_Z] \tag{5.11}$$

where F_Z represents the features obtained through computation of lower order ZM of image.

For example, an input image when subjected to NSST decomposition with $2, 2, 2$ number of directions from coarsest to finest scales, a total of 2^2=4 number of detail subbands are generated in each scale. Therefore, considering 8 different directions (θ) we obtain 8 no. of feature maps in each scale. Since (5.9) and (5.10) depends on d_L i.e. 2^{d_L} no. of subbands, thus for the given setting, the feature maps will have values ranging between [0-15] in each scale. Therefore we obtain (8×16), (8×16) and (8×16) features in scales 1, 2 and 3 respectively by encoding the detail NSST-subbands (F_1). The encoding of approximation subband using simple 'uniform' LBP scheme yields 59 features (F_2). The encoding of spatial input image using lower order ZM of order 5 provides 12 features (F_Z). Thus the feature dimension of ZM-NSST-MSLDEP for this setting is $384 + 59 + 12 = 455$.

5.1.1.5 ZM-NSST-MSLDEP based framework for image retrieval

The steps of ZM-NSST-MSLDEP feature extraction technique for retrieval of images is given below:

Algorithm: Biomedical image retrieval with proposed ZM-NSST-MSLDEP based features

Require: Input: Query image; Output: n_T number of images retrieved.

1. Load the input image
2. Obtain the shape features from spatial input image through ZMs using (5.1)
3. Apply L-level NSST on the spatial input image
4. Add non-linearity to each NSST detail subband and then normalize it to bring in the range of [0,1] and multiply it with 255 to bring it in an 8-bit range.

5. Obtain the local texture features (F_1) using proposed NSST-MSLDEP scheme using (5.10) from the NSST detail subbands

6. Obtain the local texture features (F_2) using 'uniform' LBP from the NSST approximation subband coefficients

7. Concatenate the feature vectors F_1, F_2 and F_Z obtained from Step 2, 5 and 6 respectively to form the final feature vector FV

8. Compute the distance between features of input query image and the dataset image

9. Retrieve the images in accordance to the closest matches

5.1.2 Experimental Results obtained for considered dataset

In the experiments, 3-level NSST with $2, 2, 2$ number of directions from finest to coarsest scale is used to decompose each input image. With this setting, 4 no. of detail NSST subbands in each scale and 1 no. of approximation subband is obtained. Experiments are performed on two publicly available CT image datasets and one MRI image dataset to evaluate the results of ZM-NSST-MSLDEP.

For comparison of the retrieval performance, a few well known image feature descriptors such as LDEP[200], LWP[201], LBDP[81], LBDISP[82], LBPDAP[83], CSLBCoP[114], Cont.-TrP[202], LDMaMEP[9], and LDEBP[85] are taken into consideration. The descriptors LWP, Cont.-TrP are selected for comparison because of their similar transform domain operation and competitive results. The LBDP, LBDISP and LBPDAP descriptors are well known biomedical image feature descriptors which employs bit-plane decomposition procedure. The LDEBP uses relevant global feature based ZMs and LDMaMEP employs mask based edge patterns and therefore are included for comparison purpose.

The experimental results obtained for NEMA-CT dataset is presented in Fig. 5.4(a-b) and Table 5.2. Fig. 5.4(a-b) shows % ARP, % ARR variation plots for top 10,20,30,.....50 matches of images. It is observed that for lower top matches, the performance of ZM-NSST-MSLDEP is little inferior to LBPDAP descriptor.

However, with the increasing number of top-matches the ZM-NSST-MSLDEP outperforms all the descriptors consistently. Table 5.2 shows the retrieval performance in terms of % ARP and % ARR for 40 top matches. Table 5.2 shows that at a top match 40 (in terms of % ARP), the % improvement of ZM-NSST-MSLDEP is 12 %, 9.47 %, 2.92 %, 3.37 %, 3 %, 3.91 %, 5.58 %, 4.09 % and 3.31 % over LDEP, LWP, LBDP, LBDISP, LBPDAP, CSLBCoP, Cont-TrP, LDMaMEP and LDEBP descriptors respectively. Even though the alone ZM's performance is very close to a few of the descriptors but it failed to achieve competitive performance alone. The ZM-NSST-MSLDEP with relatively less dimensions however shows improved performance over other descriptors by a good margin thus showing the effectiveness of proposed multi-feature description.

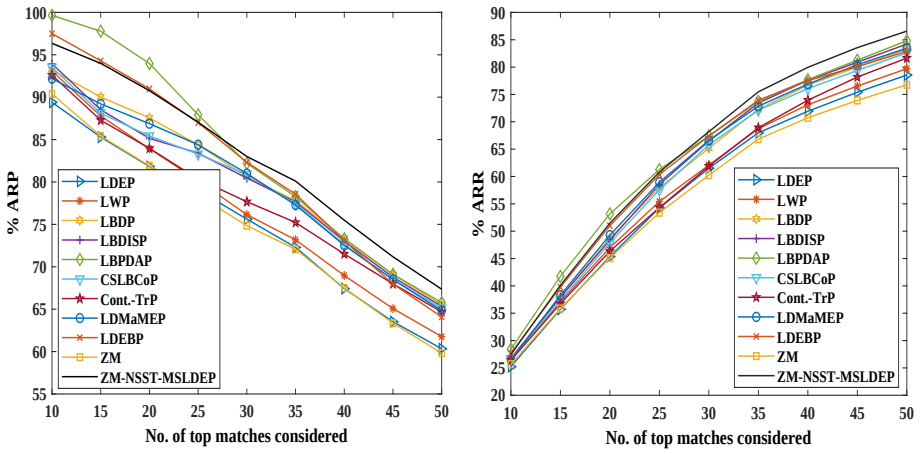

(a) (b)

Figure. 5.4: The retrieval performance comparison in terms of ARP and ARR for NEMA-CT

Table 5.2: Comparative performance evaluation of ZM-NSST-MSLDEP and other approaches in terms of % ARP and % ARR for NEMA-CT dataset(Top 40 match)

Method	LDEP[200]	LWP[201]	LBDP[81]	LBDISP[82]	LBPDAP[83]	CSLBCoP[114]	Cont.-TrP[202]	LDMaMEP[9]	LDEBP[85]	ZM only	NSST-MSLDEP
ARP	67.42	68.96	73.35	73.03	73.29	72.65	71.50	72.52	73.07	67.49	**75.49**
ARR	71.92	73.11	76.68	77.59	77.70	76.06	73.94	76.88	77.53	70.72	**79.95**

For TCIA-CT dataset, the experimental results are presented in Fig. 5.5(a-b) and Table 5.3. Fig. 5.5(a-b) plots the variation in % ARP and % ARR for 10,20,30,.....60 top match of images for TCIA-CT dataset. The ZM-NSST-MSLDEP outperforms all other descriptors consistently by a very good margin (Fig. 5.5(a-b)). Table 5.3 depicts the retrieval performance in terms of % ARP

and % ARR for 30 top matches. Table 5.3 shows that at a top match 30 (in terms of % ARP), the % improvement of ZM-NSST-MSLDEP is 29.32 %, 26.10 %, 15.96 %, 5.92 %, 3.62 %, 25.40 %, 6.78 %, 5.97 % and 2.45 % over LDEP, LWP, LBDP, LBDISP, LBPDAP, CSLBCoP, Cont.-TrP, LDMaMEP, and LDEBP descriptors respectively. For this dataset too, the ZM alone could not achieve competitive performance. However, the ZM-NSST-MSLDEP shows notable improvement over all the other descriptors including ZM alone thereby indicating the superiority of proposed shape and texture features fusion.

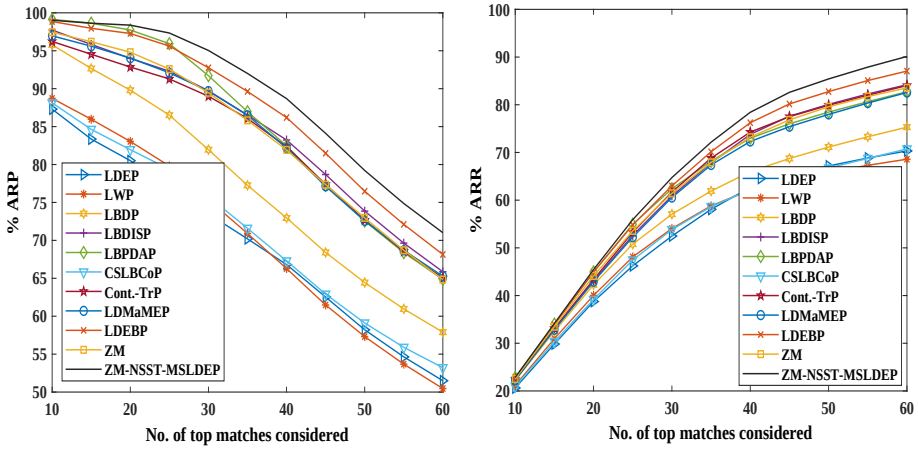

(a) (b)

Figure. 5.5: The retrieval performance comparison in terms of ARP and ARR for TCIA-CT

Table 5.3: Comparative performance evaluation of ZM-NSST-MSLDEP and other approaches in terms of % ARP and % ARR for TCIA-CT dataset (Top 30 match)

Method	LDEP[200]	LWP[201]	LBDP[81]	LBDISP[82]	LBPDAP[83]	CSLBCoP[114]	Cont.-TrP[202]	LDMaMEP[9]	LDEBP[85]	ZM only	NSST-MSLDEP
ARP	73.48	75.36	81.95	89.72	91.71	75.78	89.00	89.68	92.75	73.06	**95.03**
ARR	52.47	54.05	57.05	60.87	62.37	53.82	61.70	60.55	62.98	48.20	**64.73**

Fig. 5.6(a-b) and Table 5.4 presents the experimental results obtained in the experiments performed on York-MRI dataset. Fig. 5.6(a-b) plots the % ARP and % ARR value calculated for top match of 10,20,30,40,.....,100 images and it depicts the superiority of ZM-NSST-MSLDEP over other techniques considered for comparison. Table 5.4 tabulates the % ARP and % ARR value obtained for top match 100 images for YORK-MRI dataset. The ZM-NSST-MSLDEP shows improvement of [12.15, 12.95]%, [42.91, 45.51]%, [3.51, 3,42]%, [13.74, 14.07]%, [22.47, 21.27]%, [11.86, 11.69]%, [14.13, 15.28]%, [77.90, 76.85]%

and [39.73, 38.65]% over LDEP, LWP, LBDP, LBDISP, LBPDAP, CSLBCoP, Cont.-TrP, LDMaMEP and LDEBP respectively in terms of[ARP, ARR]%.

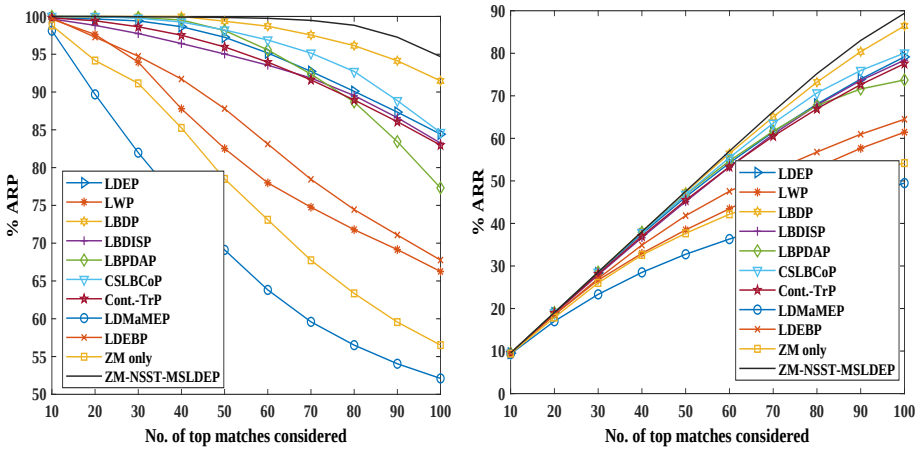

(a) (b)

Figure. 5.6: The retrieval performance comparison in terms of ARP and ARR for YORK-MRI

Table 5.4: Comparative performance evaluation of ZM-NSST-MSLDEP and other approaches in terms of % ARP and % ARR for YORK-MRI dataset (Top 100 match)

Method	LDEP[200]	LWP[201]	LBDP[81]	LBDISP[82]	LBPDAP[83]	CSLBCoP[114]	Cont.-TrP[202]	LDMaMEP[9]	LDEBP[85]	ZM only	NSST-MSLDEP
ARP	84.42	66.25	91.47	83.24	77.31	84.64	82.96	53.22	67.76	56.51	**94.68**
ARR	79.15	61.44	86.44	78.37	73.72	80.04	77.55	50.55	64.48	54.19	**89.40**

Table 5.5, tabulates the performance of the proposed ZM-NSST-MSLDEP for different scales and directions for NEMA-CT dataset. It is observed that with increase in number of scale of decomposition, the retrieval performance increases too with increase in feature dimension size. Again, the performance also depends upon number of directions considered in different scales of NSST decomposition. In order to maintain a practical balance of retrieval performance and feature dimension size, the level of NSST decomposition is set to three with [2,2,2] number of directions for NSST-MSLDEP.

The feature dimension of ZM-NSST-MSLDEP (Table 5.6) is higher than some descriptors but is quite less than many relevant descriptors too such as Cont.-TrP, LDMaMEP and CSLBCoP. In Table 5.7, the total retrieval time comparison is demonstrated. The total retrieval time is computed by evaluating the time period required for matching each dataset image with the query image and relies

Table 5.5: Performance analysis of ZM-NSST-MSLDEP for NEMA-CT dataset (top match 40) in terms of ARP and ARR for different levels of NSST decomposition and directions

Level	Direction	Total no. of subbands	ZM-NSST-MSLDEP		FD
			ARP	ARR	
1	2	1+4=5	73.02	77.38	199
2	3	1+8=9	73.30	77.59	327
	2 2	1+4+4=9	74.04	78.57	327
3	3 3	1+8+8=17	74.63	79.03	583
	2 2 2	1+4+4+4=13	75.49	79.95	455
	3 3 3	1+8+8+8=25	75.39	79.68	839

Table 5.6: Feature dimension comparison of the proposed descriptor with other techniques

Method	LDEP[200]	LWP[201]	LBDP[81]	LBDISP[82]	LBPDAP[83]	CSLBCOP[114]	Cont.-TrP[202]	LDMaMEP[9]	LDEBP[85]	ZM only	NSST-MSLDEP
Dimension	24	256	256	256	192	1024	1475	1536	85	12	455

Table 5.7: Comparative performance evaluation of ZM-NSST-MSLDEP and other approaches in terms of total retrieval time (in seconds)

Method	LDEP[200]	LWP[201]	LBDP[81]	LBDISP[82]	LBPDAP[83]	CSLBCOP[114]	Cont.-TrP[202]	LDMaMEP[9]	LDEBP[85]	ZM only	ZM-NSST-MSLDEP
NEMA-CT	0.10	0.24	0.26	0.28	0.21	0.78	1.61	2.10	0.23	0.08	0.38
TCIA-CT	0.46	1.21	1.01	1.27	1.07	3.50	8.49	9.77	0.75	0.33	1.67
YORK-MRI	0.37	0.63	0.62	0.53	0.45	1.26	3.11	4.00	0.41	0.28	0.86

on feature vector length. From Table 5.7 it is observed that the total retrieval time of ZM-NSST-MSLDEP is well faster than CSLBCoP, Cont-TrP, LDMaMEP but is slower than LDEP, LWP, LBDP, LBDISP, LBPDAP and LDEBP. However, the performance of ZM-NSST-MSLDEP is much better than LDEP, LWP, LBDP, LBDISP, LBPDAP and LDEBP descriptors.

In Fig. 5.7, the visual retrieval results are presented for all the descriptors along with the proposed approach for a particular query image from NEMA-CT dataset. It is observed that the proposed ZM-NSST-MSLDEP retrieves all the top 12 images correctly compared to the other techniques.

Figure. 5.7: Visual retrieval results (row-wise) for LDEP, LWP, LBDP, LBDISP, LBP-DAP, CSLBCoP, Cont.-TrP, LDMaMEP, LDEBP and ZM-NSST-MSLDEP descriptors, for the top 12 image matches for NEMA-CT database for a given query image. (The image enclosed inside black color rectangle is a query image. The images enclosed inside green rectangles are correctly retrieved and the images enclosed inside red rectangles are retrieved incorrectly)

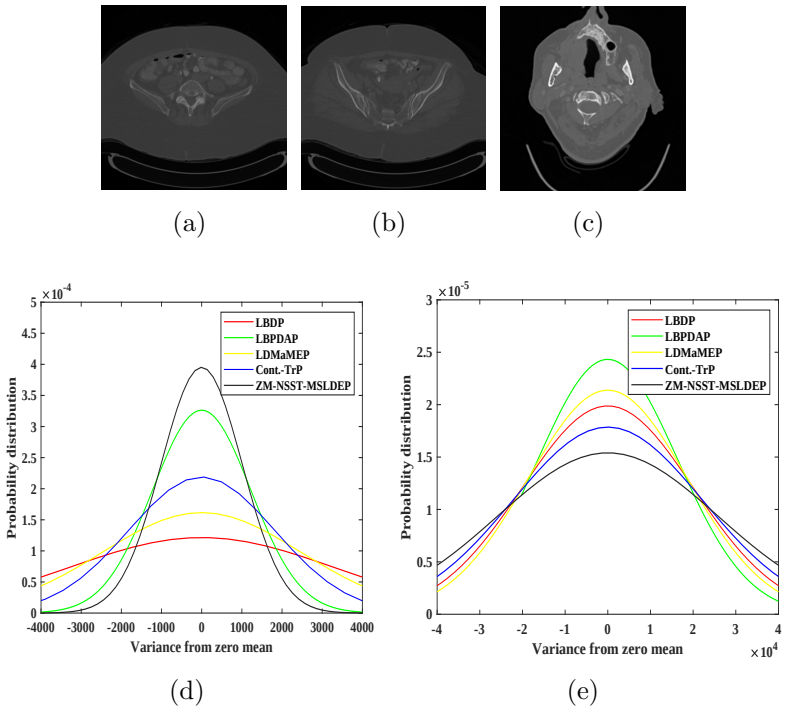

Figure. 5.8: Discriminating nature of LBDP,LBPDAP,LDMaMEP,Cont.-TrP and NSST-MSLDEP features of intra class and inter class images of TCIA-CT dataset (a) and (b) are images from same class of TCIA-CT dataset,(c) Image from different class other than (a) and (b),(d) and (e) are the pd w.r.t zero mean of difference between features from intra class and inter class images respectively

In Fig. 5.8 we show the analysis of the distinguishing behaviour of ZM-NSST-MSLDEP with respect to LBPDAP, LDMaMEP and Cont.-TrP descriptors for interclass and intraclass image examples from TCIA. The Fig. 5.8(a-b), belong to same image class and the image in Fig. 5.8(c) belongs to a different class. The Fig. 5.8(d-e) presents the p.d of intraclass and interclass feature vector difference's w.r.t zero mean for different descriptors. The high variation from zero mean indicates the lack of similarity between the features whereas the highly similar feature vectors will exhibit less variation from zero mean.

The curve corresponding to ZM-NSST-MSLDEP in Fig. 5.8(d) shows relatively much less variance from zero mean as compared to many schemes which clearly demonstrates the ZM-NSST-MSLDEPs capability of identifying the similar features belonging to the same class (intra-class). Similarly, the curve corresponding to ZM-NSST-MSLDEP in Fig. 5.8(e) shows relatively very high variance from zero mean as compared to all other schemes which clearly exhibits the ZM-NSST-MSLDEPs capability of distinguishing the inter-class images. The Fig. 5.8(d-e) confirms the remarkably high discriminative power of ZM-NSST-MSLDEP method.

5.2 Biomedical image retrieval based on ZMs and SVD-weibull distribution modelling in NSST domain

Due to presence of complicated geometrical patterns, a single feature is not enough to ensure improved feature description and often requires a combination of features for an effective image description. However the main challenge in such situations is the formation of an effective feature set without elevating the feature dimensions. In this work, we introduce a low dimensional image retrieval technique by integrating shape and texture features. The shape features in this work are described using low order ZM. The image texture features are computed from NSST approximation and detail subbands. The NSST is shift invariant, multiscale, has flexible directional selectivity and provides close to optimal approximation characteristics. An effective framework for image texture description based on NSST and singular value decomposition (SVD) is proposed. We model the pdf of the singular values of image NSST detail subband coefficients using Weibull distribution. The Weibull distribution parameters are estimated using ML estimation scheme.It is demonstrated that the singular values of the image NSST detail subband can be best approximated using Weibull distribution compared to GGD and exponential. This new feature descriptor is referred to as ZM-NSST-SVDw descriptor.

5.2.1 Methodology

This section presents the proposed ZM-NSST-SVDw descriptor in detail. The block diagram of ZM-NSST-SVDw is shown in Fig. 5.9.

The complete ZM-NSST-SVDw computation process is divided into a few main steps like: ZM computation, NSST decomposition, non-linearity addition, encoding of NSST detail subbands using statistical modeling of its singular values, encoding of NSST approximation subband using simple LBP ‘uniform’ pattern, subband mean and standard deviation, and final feature vector computation.

The description on ZMs computation and LBP ‘uniform’ computation is provided in the previous section of this chapter whereas the explanation on NSST decomposition and non-linearity addition are provided in the previous chapters.

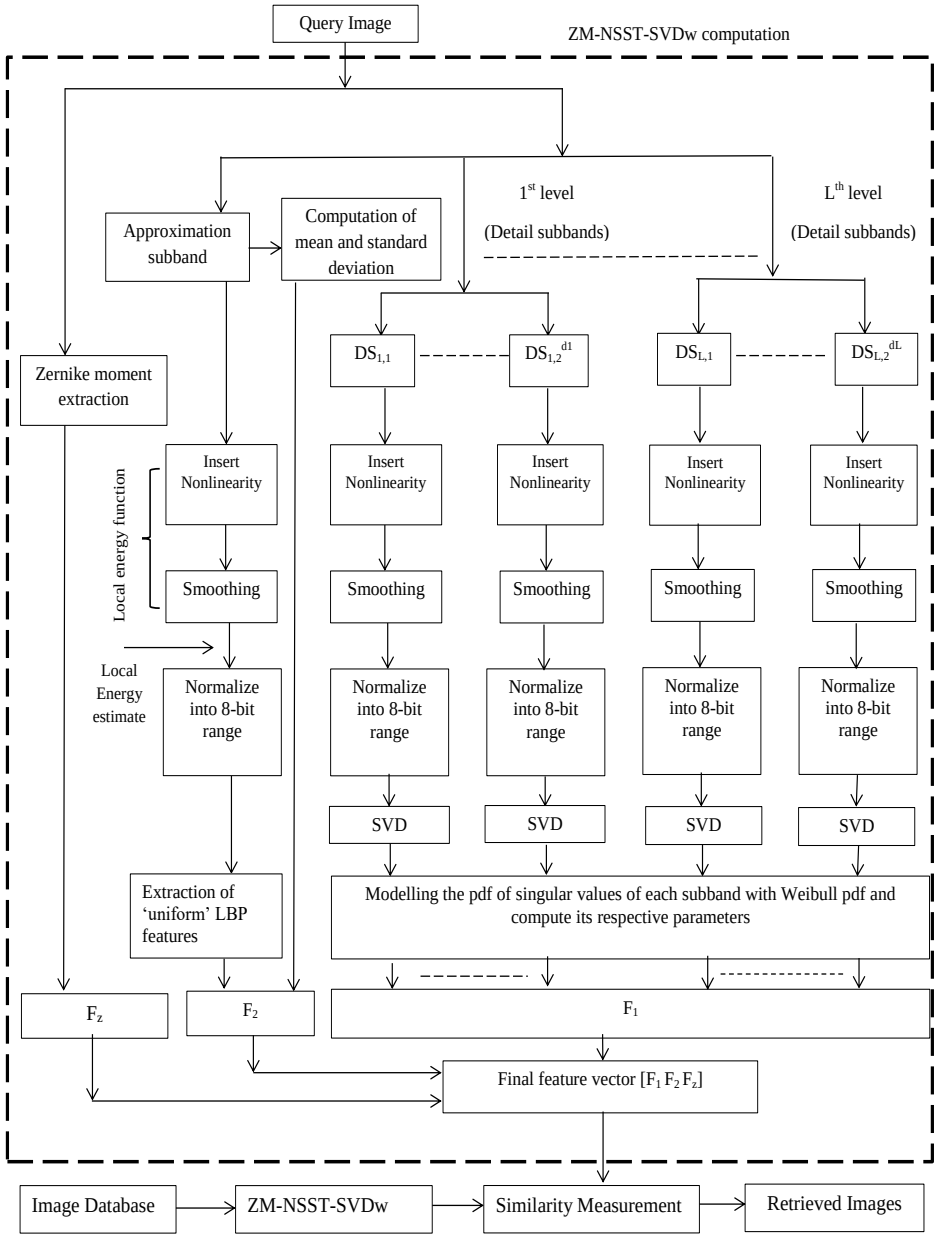

Figure. 5.9: Block diagram of ZM-NSST-SVDw descriptor in an image retrieval framework

5.2.1.1 Texture feature extraction from image NSST detail subbands by modelling the singular values obtained from singular value decomposition

The ZM-NSST-SVDw descriptor approximates the singular values obtained from singular value decomposition (SVD) of image NSST detail subbands by using Weibull distribution. The parameters of Weibull distribution are considered as global features because they serve the image signal as a full and captures the overall statistical distribution of the data inside it. The details are presented

below.

5.2.1.2 Singular value decomposition (SVD)

SVD is an image transformation approach used in many applications such as image denoising [209,210], watermarking [211–213],compression [214], classification [196] and retrieval [215] etc. SVD applied on image I of size $M \times N$ decomposes it into three matrices given as-

$$I_s = USV^{-1} \tag{5.12}$$

where U and V are orthogonal matrices of size $M \times M$ and $N \times N$ respectively. S is a diagonal matrix with non-negative diagonal entries ordered in decreasing order of magnitude shown in (5.13). The values $\sigma_{s1}, \sigma_{s2}, ...\sigma_{sn}$ in S are known as singular values for the decomposition. These singular values are the square roots of the respective eigen values of the matrix $I_s I_s^T$.

$$S = \begin{bmatrix} \sigma_{s1} & 0 & 0 & \dots & 0 & 0 \\ 0 & \sigma_{s2} & 0 & \dots & 0 & 0 \\ \vdots & & & & & \\ 0 & 0 & 0 & \dots & 0 & \sigma_{sn} \end{bmatrix} \tag{5.13}$$

5.2.1.3 Statistical modelling of pdf of singular values

Usually, the pdf of the image NSST coefficients are modelled directly using various statistical models. However due to the involvement of large number of NSST coefficients the parameter estimation of statistical model becomes computationally expensive. The singular values obtained after applying SVD on NSST subbands are much less in numbers as compared to the no. of NSST coefficients in a subband. In [196] Selvan and Ramakrishnan modeled the singular values of image wavelet coefficients using exponential distribution for texture classification in order to save computations. Motivated from [196], we investigate the statistics of singular values of image NSST coefficients for various types of CT and MRI images. We observe that the statistics of singular values of image NSST coefficients varies from image to image. It was also observed that for the same image, the subband statistics at all the scales varies among each other. It clearly indicates that the singular values

Table 5.8: The estimated parameters of fitted models of the singular values of NSST subband coefficients (2,2 NSST decomposition) for an image from TCIA-CT dataset

Subband	GGD			Weibull		Exponential
	mean	scale	shape	scale	shape	mean
S11	23.38	19.05	0.71	1.07	0.24	23.38
S12	31.28	25.06	0.72	2.18	0.27	31.28
S13	27.15	20.18	0.68	1.26	0.28	27.15
S14	34.36	28.12	0.72	3.29	0.31	34.36
S21	16.98	14.39	0.77	4.49	0.39	16.98
S22	20.33	16.11	0.75	6.26	0.43	20.33
S23	21.09	13.02	0.68	5.26	0.42	21.09
S24	19.85	15.41	0.75	7.12	0.45	19.85

can provide good discrimination between the images.

Fig. 5.10, shows the plots of empirical pdf's of various image NSST subbands and the GGD, Exponential and Weibull pdf's fitted to it. It is further seen that the Weibull pdf provides the best fit to the empirical pdf. We achieve the similar outcomes for other images too. The parameters of GGD, Weibull and Exponential distributions are estimated using ML approach. The example of estimated parameters of GGD, Weibull and exponential distributions for various subbands of a CT image is provided in Table 5.8. It can be clearly observed that the distribution parameters vary from subband to subband indicating about the discriminating information each subband carries.

Weibull distribution

Weibull distribution is a continuous pdf and has been widely used in different applications [216]. The expression for two parameter Weibull distribution for random variable 'r' is given as

$$F(r) = \frac{\nu}{\eta}(\frac{r}{\eta})^{\nu-1} exp(-(\frac{r}{\eta})^{\nu}) \tag{5.14}$$

$\nu > 0$ and $\eta > 0$ are the shape and scale parameter respectively. These two parameters are estimated with ML estimation technique [217].

The NSST approximation subband is encoded using 'uniform' LBP features, subband mean and subband standard deviation to form F_2 features.

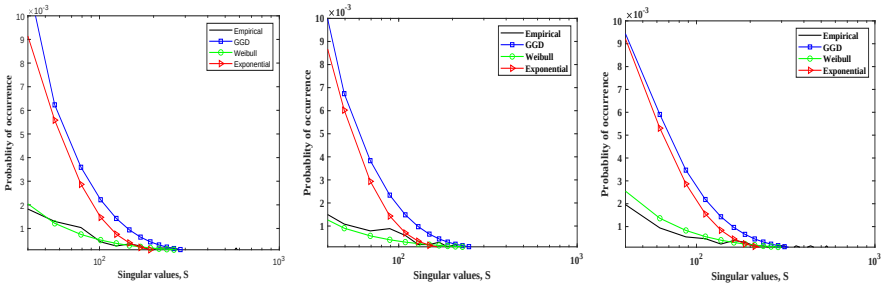

(a) Image 1

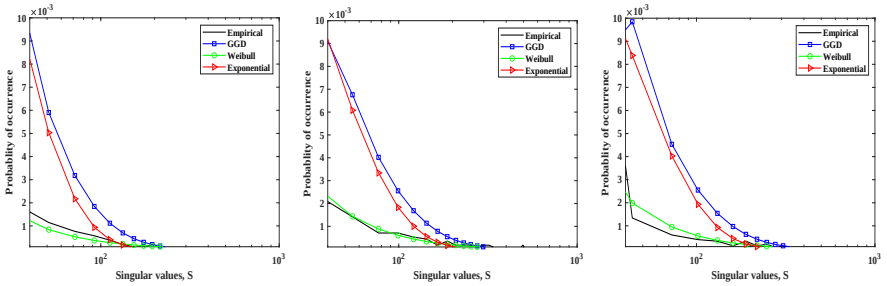

(b) Image 2

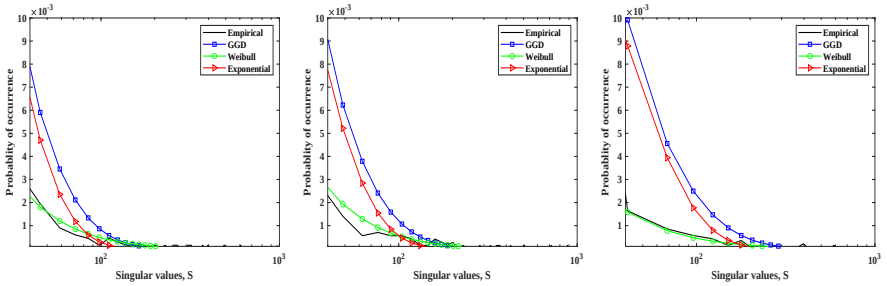

(c) Image 3

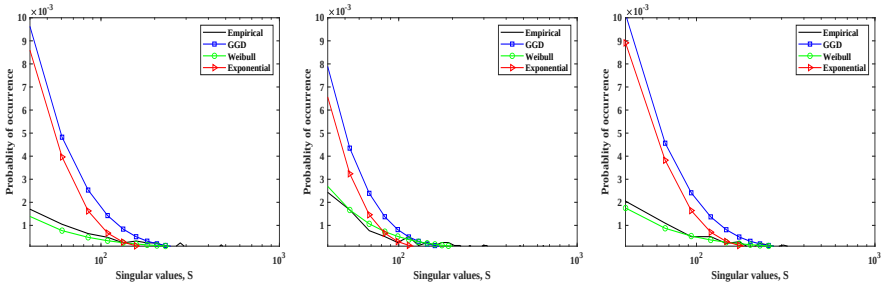

(d) Image 4

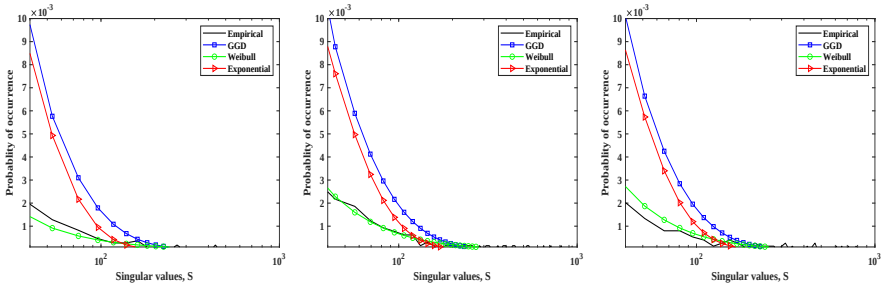

(e) Image 5

Figure. 5.10: Log histograms for three detail NSST subbands for five different images of TCIA-CT dataset and the generalized Gaussian, Exponential and Weibull distribution fitted to these histograms.

5.2.1.4 Formation of final feature vector

The final feature vector (FV) is formed by combining the features F_1, F_2 and F_z as

$$FV = [F_1, F_2, F_z] \tag{5.15}$$

where F_z denotes the global shape features computed using low order ZM. If we consider a 3 level NSST decomposition with 2,3,4 directions from coarsest to finest, a total of 28 detail subbands are obtained. Therefore, $F_1 = 28 \times 2 = 56$ features are obtained from detail subbands. The approximation subband is encoded using 'uniform' LBP features (59 features), approximation subband mean and standard deviation (2 features), thus $F_2 = 59 + 2 = 61$ features. To form F_z, we employed 5^{th} order ZM features i.e. $F_z = 12$ features are obtained. Therefore, $FV_{=}61 + 56 + 12 = 129$ features are obtained.

The steps involved in ZM-NSST-SVDw based feature extraction in an image retrieval framework are:

Algorithm: Biomedical image retrieval with proposed ZM-NSST-SVDw feature descriptor

Require: Input: Query image; Output: n_T' number of images retrieved.

1. Load the input image.
2. Use lower order ZM to extract shape features from an input image in spatial domain.
3. Apply NSST on the input grayscale image.
4. Incorporate the non-linearity to each NSST subband
5. Obtain the texture features using Weibull distribution parameters estimated from the singular values obtained after applying SVD on the NSST detail subbands.
6. Obtain local texture features using 'uniform' LBP from the approximation subband.

7. Construct the final feature vector by considering the feature obtained from the steps 2, 5 and 6.
8. Compute the similarity between features of query image and the database images
9. Retrieve the most relevant images according to the distance calculated

---

5.2.2 Experimental Results obtained for considered datasets

This section provides the discussion on experimental results to analyse the performance of ZM-NSST-SVDw features in a CBIR framework.

For the experiments, three level of NSST decomposition with 2,3,4 number of directions from coarsest to finest scale are considered to decompose the images. It results into one NSST approximation subband and a total of $2^2 + 2^3 + 2^4 = 4 + 8 + 16 = 28$ number of NSST detail subbands.

For the performance evaluation of ZM-NSST-SVDw descriptor, the comparison is done with a few of the existing state of the art hand-crafted techniques for biomedical image retrieval. They are LDEP[200], LWP[201], LBDP, LBDISP [82], LBPDAP [83], CSLBCoP[114], Cont.-TrP[202], LDMaMEP[9] and LDEBP [85].

To analyse the performance of ZM-NSST-SVDw in comparison to other existing techniques, experiments are performed on NEMA-CT dataset. Every image in the dataset is considered as a query, and the performance for top matches of 10, 20,....50, are calculated. The ARP and ARR value computed for these top matches can be observed in Fig. 5.11(a-b). The low dimensional ZM-NSST-SVDw, consistently outperforms, LDEP, LWP, LBDP, LBDISP, LBPDAP, CSLBCoP, Cont.-TrP, LDMaMEP and ZM descriptors in all the top matches. Table 5.9 presents the % ARP and % ARR values of ZM-NSST-SVDw and all other techniques for a top match of 40 images. The ZM-NSST-SVDw shows superior performance as compared to all the other state of the art descriptors at a top match of 40. The ZM-NSST-SVDw shows 11.94%, 9.44 % ,2.89 % , 3.34%, 2.97%, 3.88%, 5.55 %, 4.07 % and 3.28 % improvement over LDEP, LWP, LBDP, LBDISP, LBPDAP, CSLBCoP, Cont.-TrP, LDMaMEP, and LDEBP respectively in

terms of ARP where as the proposed descriptor shows improvement of 11.37 %, 9.56 %, 4.46%, 3.23%, 3.09%, 5.31 %, 8.33 %, 4.19 % and 3.31% over LDEP, LWP, LBDP, LBDISP, LBPDAP, CSLBCoP, Cont.-TrP, LDMaMEP,and LDEBP respectively in terms of ARR. The ZM-NSST-SVDw exhibits consistently superior performance at increasing number of top matches for NEMA-CT database. The shape features alone using ZM shows comparable results with LDEP and LWP descriptors but underperforms all other descriptors by a high margin which clearly demonstrate the need of multiple feature description in order to better discriminate between different classes. The ZM-NSST-SVDw even outperformed recent LDEBP descriptor which is also based on the multiple feature combination.

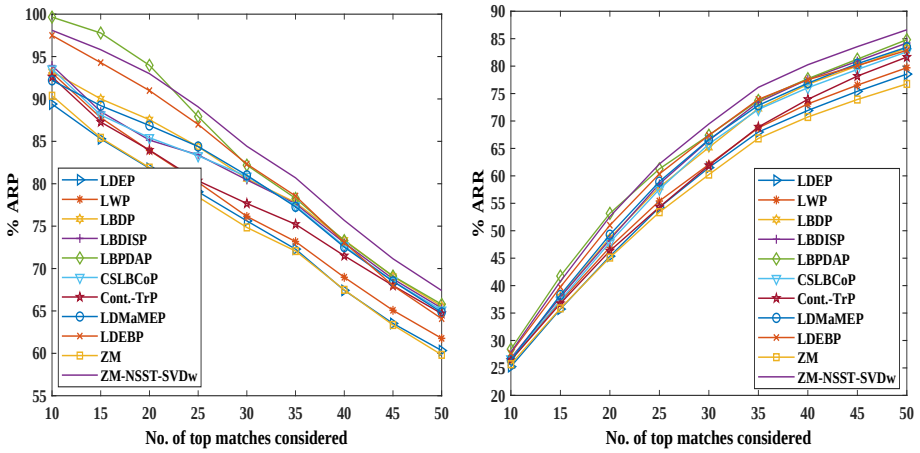

(a) (b)

Figure. 5.11: The retrieval performance comparison in terms of (a)ARP and (b)ARR for NEMA-CT

Table 5.9: Comparative performance evaluation of ZM-NSST-SVDw and other approaches in terms of % ARP and % ARR for NEMA-CT dataset(Top 40 match)

Method	LDEP[200]	LWP[201]	LBDP[81]	LBDISP[82]	LBPDAP[83]	CSLBCoP[114]	Cont.-TrP[202]	LDMaMEP[9]	LDEBP[85]	ZM only	ZM-NSST-SVDw
ARP	67.42	68.96	73.35	73.03	73.29	72.65	71.50	72.52	73.07	67.49	**75.47**
ARR	71.92	73.11	76.68	77.59	77.70	76.06	73.94	76.88	77.53	70.72	**80.10**

The experimental results for TCIA-CT dataset are presented in Fig. 5.12 and Table 5.10. The % ARP and % ARR has been calculated for different top match of images and presented in Fig. 5.12(a-b). The % ARP and % ARR curves presented in Fig. 5.12(a-b) distinctly shows the superiority of ZM-NSST-SVDw over others for the different top matches considered. The Table 5.10 depicts the % ARP and % ARR values obtained for maximum of 30 top match

of images. The ZM-NSST-SVDw shows improvement over LDEP, LWP, LBDP, LBDISP, LBPDAP, CSLBCoP, Cont.-TrP, LDMaMEP, and LDEBP by a margin of ,[29.79,23.59]%, [26.55,19.98]%, [16.38,13.67]%, [06.30,06.54]%, [03.99,03.98]%, [25.85,20.49]%, [07.16,05.11]%, [06.34,07.10]%, and [02.82,02.97]% in terms of [ARP,ARR]% at top match of 30. The ZM-NSST-SVDw descriptor consistently outperforms all the other descriptors both in terms of % ARP and % ARR (Table 5.10). Although ZM descriptor alone performs better than some descriptors but fails to achieve satisfactory performance in many situations which again calls for the need of multiple feature description in order to better discriminate between classes. The results of ZM-NSST-SVDw clearly indicates that with even low dimensions the proposed ZM-NSST-SVDw can outperform the popular bit plane based methods, multiple feature based descriptors and various transform based descriptors.

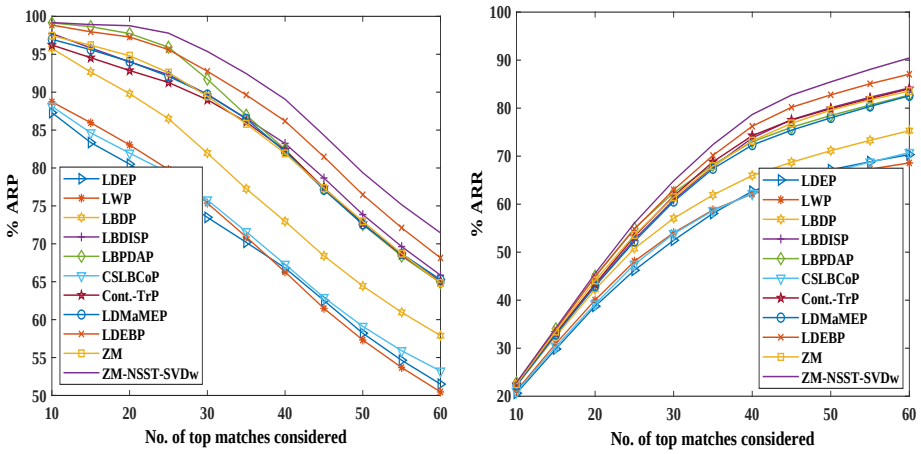

(a) (b)

Figure. 5.12: The retrieval performance comparison in terms of (a)ARP and (b)ARR for TCIA-CT

Table 5.10: Comparative performance evaluation of ZM-NSST-SVDw and other approaches in terms of % ARP and % ARR for TCIA-CT dataset (Top 30 match)

Method	LDEP[200]	LWP[201]	LBDP[81]	LBDISP[82]	LBPDAP [83]	CSLBCoP[114]	Cont.-TrP[202]	LDMaMEP[9]	LDEBP[85]	ZM only	ZM-NSST-SVDw
ARP	73.48	75.36	81.95	89.72	91.71	75.78	89.00	89.68	92.75	89.46	**95.37**
ARR	52.47	54.05	57.05	60.87	62.37	53.82	61.70	60.55	62.98	61.44	**64.85**

The % ARP and % ARR values computed for different top match of images for York-MRI dataset is presented in Fig. 5.13(a-b). It has been clearly

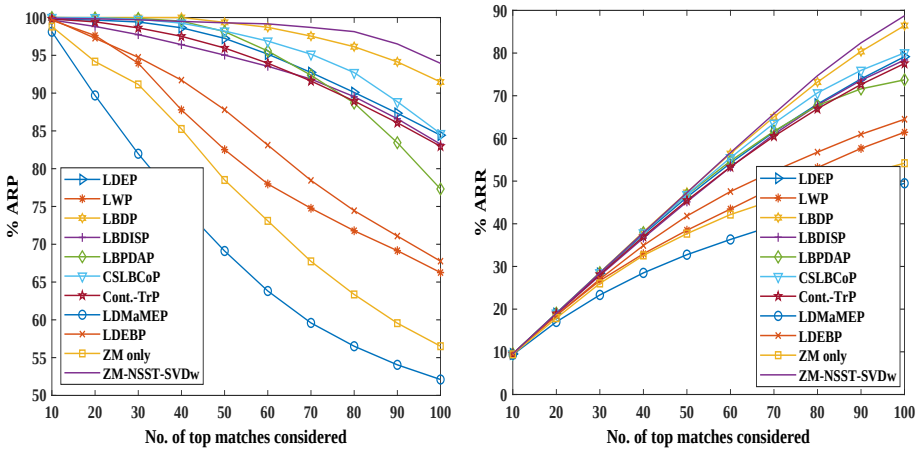

(a) (b)

Figure. 5.13: The retrieval performance comparison in terms of (a)ARP and (b)ARR for YORK-MRI

Table 5.11: Comparative performance evaluation of ZM-NSST-SVDw and other approaches in terms of % ARP and % ARR for YORK-MRI dataset (Top 100 match)

Method	LDEP[200]	LWP[201]	LBDP[81]	LBDISP[82]	LBPDAP[83]	CSLBCoP[114]	Cont.-TrP[202]	LDMaMEP[9]	LDEBP[85]	ZM only	ZM-NSST-SVDw
ARP	84.42	66.25	91.47	83.24	77.31	84.64	82.96	53.22	67.76	56.51	**93.94**
ARR	79.15	61.44	86.44	78.37	73.72	80.04	77.55	50.55	64.48	54.19	**88.75**

observed that the ZM-NSST-SVDw outperforms the other techniques with significant margins with less feature dimension for different top matches. Table 5.11 presents the % ARP and % ARR values obtained for top match of 100 images. ZM-NSST-SVDw outperforms LDEP, LWP, LBDP, LBDISP, LBPDAP, CSLBCOP, Cont.-TrP, LDMeMEP and LDEBP by [11.27,12.12]%,[41.79, 44.44]%,[2.70,2.67]%,[12.85,13.24]%,[21.51,20.38]%,[10.98,10.88]%,[13.23,14.44]%, [76.51,75.56]% and [38.63,37.63]% in terms of [ARP, ARR]%. ZM-NSST-SVDw shows better retrieval performance with less feature dimension compared to other high dimensional feature descriptors such as LWP, LBDP, LBDISP, LBPDAP, CSLBCoP, Cont.-TrP and LDMaMEP.

Table 5.12 presents the feature vector dimension comparison of ZM-NSST-SVDw descriptor and other state of the art handcrafted descriptors. The ZM-NSST-SVDw descriptor, exhibits the lowest dimension among all the other descriptors except LDEP and LDEBP. However the performance of proposed ZM-NSST-SVDw is much superior to these two methods and exhibits consistently

Table 5.12: Feature dimension comparison of the proposed descriptor with other techniques

Method	LDEP[200]	LWP[201]	LBDP[81]	LBDISP[82]	LBPDAP [83]	CSLBCOP[114]	Cont.-TrP[202]	LDMaMEP[9]	LDEBP[85]	ZM only	ZM-NSST-SVDw
Dimension	24	256	256	256	192	1024	1475	1536	85	12	129

superior performance at increasing number of top matches for all the datasets considered for experiments.

Table 5.13: Comparative performance evaluation of ZM-NSST-SVDw and other approaches in terms of total retrieval time (in seconds)

Method	LDEP[200]	LWP[201]	LBDP[81]	LBDISP[82]	LBPDAP [83]	CSLBCOP[114]	Cont.-TrP[202]	LDMaMEP[9]	LDEBP[85]	ZM only	ZM-NSST-SVDw
NEMA-CT	0.10	0.24	0.26	0.28	0.21	0.78	1.61	2.10	0.23	0.08	0.17
TCIA-CT	0.46	1.21	1.01	1.27	1.07	3.50	8.49	9.77	0.75	0.33	0.72
YORK-MRI	0.37	0.63	0.62	0.53	0.45	1.26	3.11	4.00	0.41	0.28	0.40

Table 5.13 shows the total retrieval time (in seconds) comparison of the ZM-NSST-SVDw descriptor with other descriptors. We calculate the total retrieval time by estimating the time required to match the query with each database image which depends on mainly on feature vector dimensions. It is observed that the proposed descriptor possess the lowest total retrieval time for the datasets considered for experiments in comparison with all other techniques considered.

The Fig. 5.14 presents the visual retrieval results obtained for an image taken from NEMA-CT dataset. It is clearly observed that the proposed descriptor retrieves all the top 15 match of images correctly as compared to existing techniques considered for comparison.

The Fig. 5.15 demonstrates ZM-NSST-SVDw's ability to discriminate between classes of images from the TCIA-CT database using LBDP, LBPDAP, LDMaMEP, Cont.-TrP, and NSST-LBNDP. Fig. 5.15(a) and (b) belongs to same class of image and 5.15(a)and(c) belongs to different classes. The Fig.s 5.15(d-e) displays the p.d. of the intraclass and interclass feature vector differences with respect to the zero mean for various descriptors. The lack of similarity between the features is indicated by their considerable variance from zero mean, but the

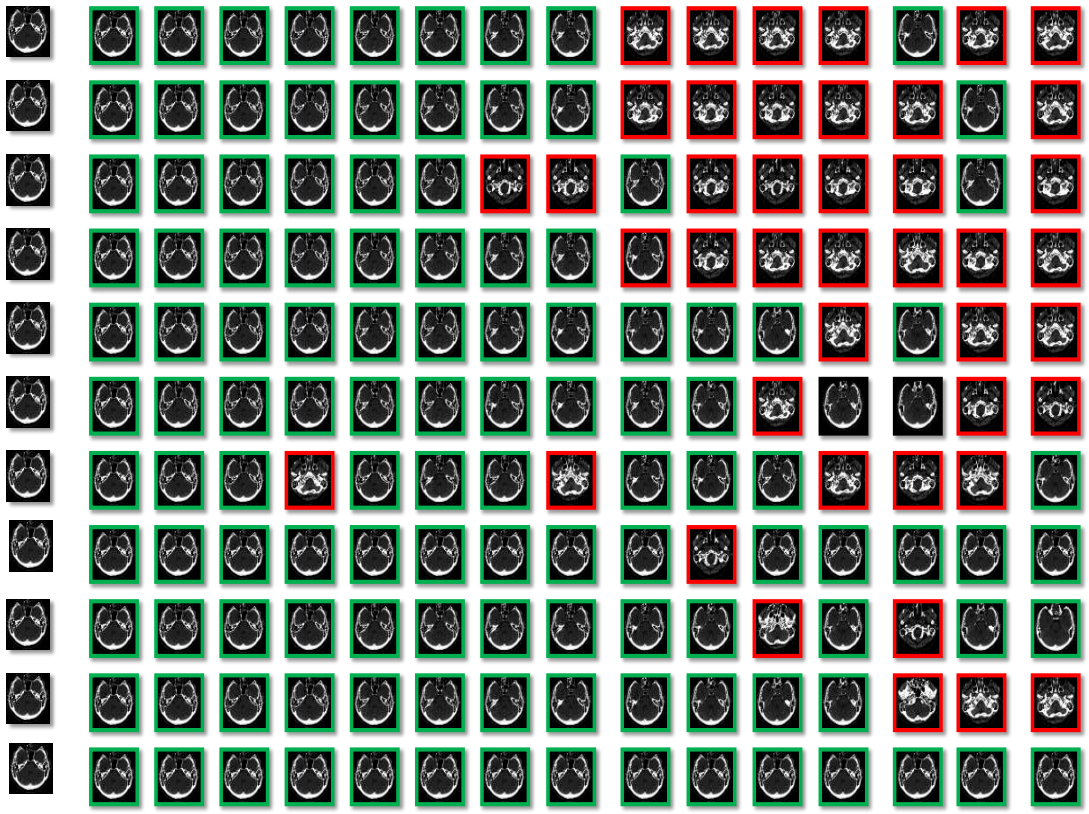

Figure. 5.14: Visual retrieval results for LDEP, LWP, LBDP, LBDISP, LBPDAP, CSLBCoP, Cont.-TrP, LDMaMEP, LDEBP, NSST-LBNDP and ZM-NSST-SVDw descriptors (from top most row to last row), for the top 15 image matches for NEMA-CT database for a given query image. (The leftmost image is a query image, while the images inside red boxes were retrieved incorrectly)

feature vectors' higher similarity is indicated by their bigger amplitudes relative to zero mean. Fig.s 5.15(d-e) show that the proposed descriptor has noticeably strong discriminative power for identifying intraclass images and inter class images.

5.3 Comparison of all the proposed NSST domain feature descriptors for biomedical image retrieval

In this section, the retrieval performance comparison of all the biomedical image feature descriptors introduced in this thesis are presented. For quantitative performance analysis, % ARP and % ARR are considered as evaluation parameters. Also, the comparison analysis of total retrieval time and feature dimension are included.

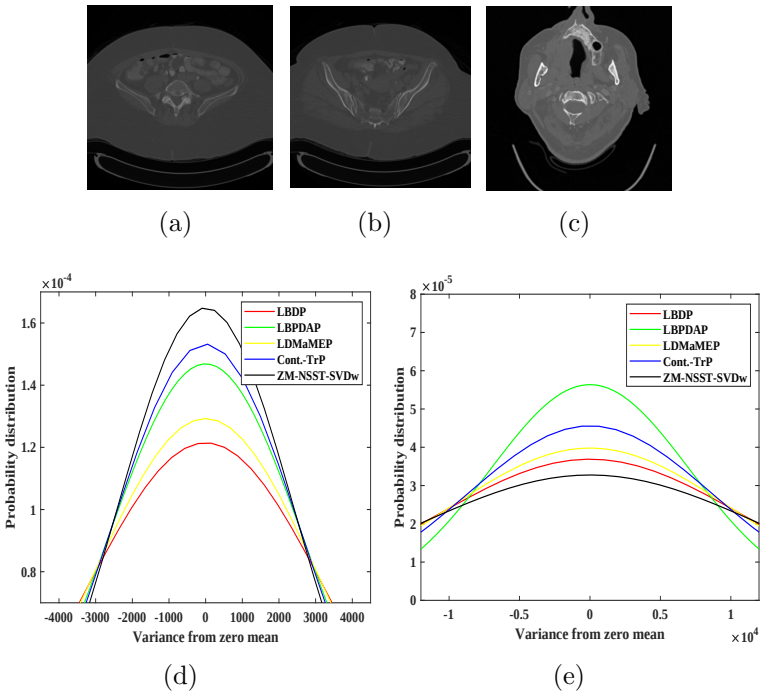

Figure. 5.15: Discriminating nature of LBDP,LBPDAP,LDMaMEP,Cont.-TrP, NSST-LBNDP and Proposed features of intra class and inter class images of TCIA-CT dataset (a) and (b) are images from same class of TCIA-CT dataset,(c) Image from different class other than (a) and (b),(d) and (e) are the probability distribution w.r.t zero mean of difference between features from intra class and inter class images respectively

Fig. 5.16, presents the retrieval performance comparison in terms of % ARP and % ARR, for different top match of images for NEMA-CT, TCIA-CT and YORK-MRI dataset. From these curves, the following inferences are observed.

- For NEMA-CT dataset, the NSST-LBNDP perform superior to, NSST-LBPDAP, ZM-NSST-SVDw and ZM-NSST-MSLDEP in terms of % ARP (Fig. 5.16(a)). In terms of % ARR, NSST-LBNDP shows close performance with NSST-LBPDAP for lower top matches, but shows improvement for higher top matches. NSST-LBNDP is observed to perform better compared to ZM-NSST-MSLDEP and ZM-NSST-SVDW consistently (5.16(b)).

- For TCIA-CT dataset, ZM-NSST-SVDw shows superior results compared to NSST-LBPDAP and NSST-LBNDP for all the top matches considered however performs pretty close to ZM-NSST-MSLDEP (Fig. 5.16(c)) in terms of % ARP. In terms of % ARR, the ZM-NSST-SVDw is observed to perform almost close to ZM-NSST-MSLDEP throughout all the top matches considered. However, ZM-NSST-SVDw has shown superior results compared to bit-plane based approaches NSST-LBPDAP and NSST-LBNDP almost consistently which can be clearly seen in Fig. 5.16(d).

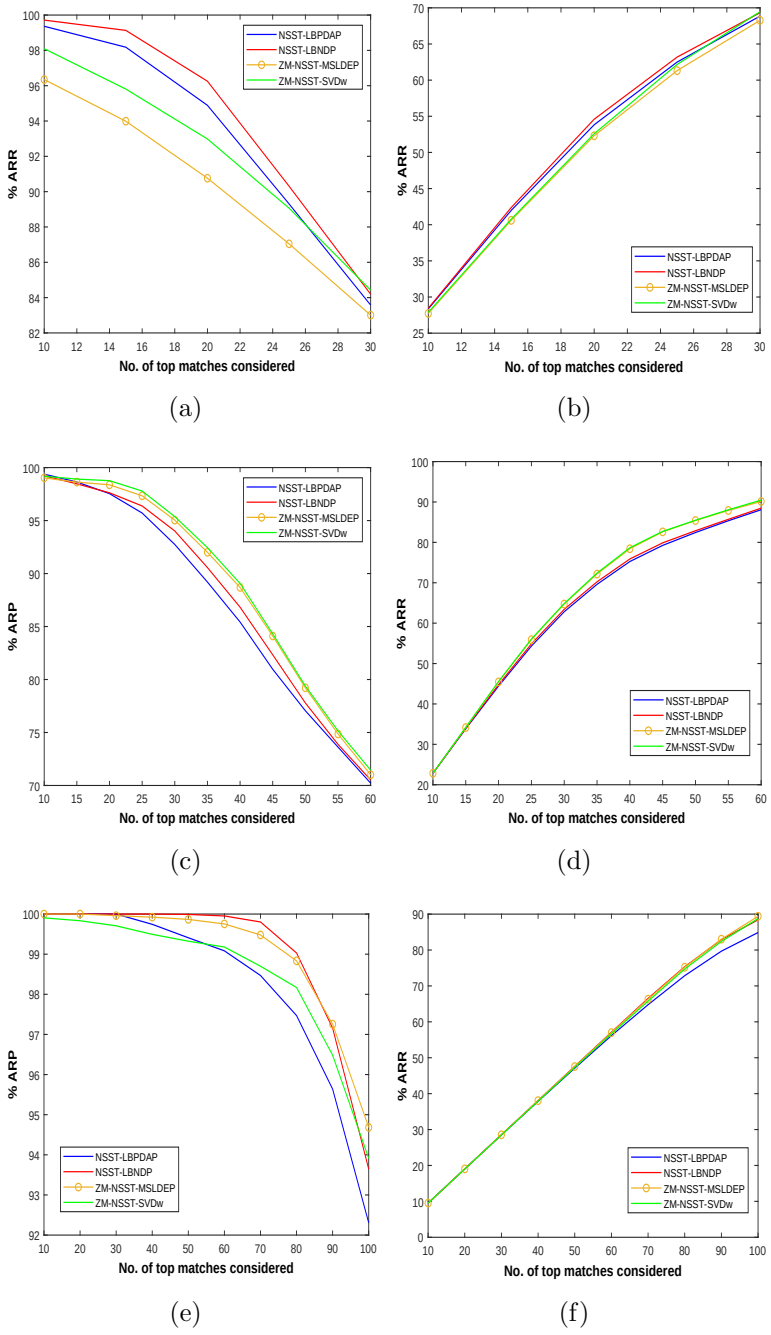

Figure. 5.16: The retrieval performance comparison of NSST-LBPDAP, NSST-LBNDP, ZM-NSST-MSLDEP and ZM-NSST-SVDw in terms of ARP and ARR for (a)NEMA-CT, (b)TCIA-CT, (c)YORK-MRI

- Fig. 5.16(e-f) presents the plots for % ARP and % ARR, computed for different top matches for YORK-MRI dataset. NSST-LBNDP shows superior performance upto top match of 90 in terms of % ARP compared to ZM-NSST-MSLDEP, ZM-NSST-SVDw and NSST-LBPDAP. However, ZM-NSST-MSLDEP, performs better after top match of 90 images (5.16(e)). In terms of % ARR, NSST-LBNDP, ZM-NSST-MSLDEP, ZM-NSST-SVDw

and NSST-LBPDAP shows quite similar performance upto top match of 60 images, however the other three techniques overcomes NSST-LBPDAP for higher top matches(5.16(f)).

Table 5.14: Feature dimension and total retrieval time (in seconds) comparison of all the proposed biomedical image feature descriptors

Method	NSST-LBPDAP	NSST-LBNDP	ZM-NSST-MSLDEP	ZM-NSST-SVDw
NEMA-CT	2.34	0.44	0.38	0.17
TCIA-CT	16.96	2.19	1.67	0.72
YORK-MRI	3.52	0.99	0.86	0.40
FD	1728	596	455	129

From Table 5.14, we observe that the ZM-NSST-SVDw has the least and NSST-LBPDAP posses the highest feature dimension. In terms of total retrieval time, ZM-NSST-SVDw is the fastest among all the descriptors proposed for biomedical image retrieval in this thesis. ZM-NSST-SVDw with very less feature dimension is observed to have shown promising performance for most of the considered datasets thereby indicating the efficacy of blend of texture and shape features.

5.4 Summary

In this chapter, two descriptors for biomedical image retrieval are presented which considers both shape and texture features. The first one extracts shape features from spatial image and the local texture features are extracted from NSST domain. One new approach for extraction of local texture features, NSST-MSLDEP is introduced here. In NSST-MSLDEP, for a subband, edge information w.r.t to a given reference is calculated for $\theta = [0°, 45°, 90°, 135°, 180°, 225°, 270°, 315°]$ directions. With these edge values computed for a particular direction θ, maximum to minimum subband edge distribution are obtained with the detail subbands in a particular scale. After which pattern maps are computed for each of the scale using sign of directional edges. The approximation subband is encoded using 'uniform' LBP. The texture information from NSST subbands and the ZM feature obtained from spatial image, together form ZM-NSST-MSLDEP descriptor. This descriptor provides discriminative information of an image with complementary shape and texture details. ZM-NSST-MSLDEP captures from both intra and inter subband details and provide discriminative information from images which increases the retrieval performance which is observed from the experimental results obtained.

The maintenance of a practical balance of retrieval performance of a CBIR framework without much increase in feature dimension is crucial. To address this issue, in the second work, another feature descriptor is introduced by combining the shape and texture features. The shape features are extracted using low order ZM and texture features are extracted in NSST domain. Here the singular values obtained from SVD of an image NSST detail subbands is modelled using Weibull distribution. Weibull distribution is found to provide accurate fit to the distribution of singular values as compared to Exponential and generalized Gaussian distributions. The parameters of Weibull distribution from image detail NSST subbands, low order ZM from spatial image and texture information in the form of 'uniform' LBP features along with mean and standard deviation computed from image NSST approximation subband are fused together to form ZM-NSST-SVDw descriptor. The parameter estimation of Weibull distribution of singular values is less computationally complex compared to estimating distribution parameters directly from individual subbands. It has shown improved performance with less feature dimensions and significantly less total retrieval time compared to many of the existing techniques.